

# Co-Optimization of Network Topology and Variable Impedance Devices under Dynamic Line Ratings in Power Transmission Systems

Junseon Park<sup>\*§</sup>, Hyeonon Park<sup>\*</sup>, Rahul K. Gupta<sup>§</sup>

<sup>\*</sup>Pukyong National University, Busan, South Korea, <sup>§</sup>Washington State University, Pullman, WA, USA.

Abstract—Power system operators are increasingly deploying Grid Enhancing Technologies (GETs) to mitigate operational challenges such as line and transformer congestion, and voltage violations. These technologies, including Network Topology Optimization (NTO), Variable Impedance Devices (VIDs), and Dynamic Line Rating (DLR), enhance system flexibility and enable better utilization of existing network assets. However, as the deployment of multiple GETs grows, effective coordination among them becomes essential to fully realize their potential benefits. This paper presents a co-optimization framework that models and coordinates NTO, VID, and DLR within a unified optimization scheme to alleviate network congestion and minimize operational costs. The NTO formulation is developed using a node-breaker model, offering finer switching granularity and improved operational flexibility. The inclusion of VIDs introduces nonlinear and non-convex relationships in the optimization problem. DLR takes into account of weather conditions, primarily wind speed and ambient temperature, enabling adaptive utilization of transmission capacity. The proposed framework is validated on standard IEEE benchmark test systems, demonstrating its effectiveness under varying numbers and placements of impedance controllers.

Index Terms—Grid enhancing technologies, Network topology optimization, Dynamic line rating, Variable impedance devices.

## Nomenclature

### Indices

$l$	Index for the lines
$e$	Index for the {from, to} end of the line $e \in \{fr, to\}$
$t$	Index for the times
$b$	Index for the substations
$g$	Index for the generators
$d$	Index for the load demands
$i$	Index for the busbar $i \in \{1, 2\}$

### Sets

$G_b$	Set of the generators in substation $b$
$D_b$	Set of the loads in substation $b$

$LF_b$	Set of the transmission lines whose directions of power flow are from substation $b$
$LT_b$	Set of the transmission lines whose directions of power flow are to substation $b$

### Parameters

$\bar{b}_l$	Nominal susceptance of the line $l$ [S]
$T_{avg}$	Average temperature of conductor [°C]
$R(T_{avg})$	Conductor resistance at $T_{avg}$ [ $\Omega$ ]
$mC_p$	Total heat capacity of conductor [J/(m·°C)]
$q_c$	Convection heat loss rate per unit length [W/m]
$q_s$	Heat gain rate from sun [W/m]
$q_r$	Radiated heat loss rate per unit length [W/m]
$\alpha^{DLR}$	DLR capacity factor, defined as the ratio of current under DLR to that under SLR.
$\theta^{max}$	Maximum allowed voltage angle [rad]
$P_g^{min}$	Lower limits for power generation of generator $g$ [MW]
$P_g^{max}$	Upper limits for power generation of generator $g$ [MW]
$P_d^{max}$	Maximum amount of load demand $d$ [MW]
$I$	Conductor line rating [A]
$M$	A sufficiently great number
$r$	Susceptance change rate
$c_{g,2}/c_{g,1}/c_{g,0}$	Cost coefficient of generator $g$
$N_g$	Number of generators
$N_b$	Number of buses
$VOLL$	Value of Lost Load [\$/MWh]

### Continuous Variables

$P_l$	Power flow on line $l$ [MW]
$P_{g,i}$	Generation power connected to busbar $i$ [MW]
$P_{d,i}$	Load demand connected to busbar $i$ [MW]
$P_{l,e,i}$	Line power flow on line $l$ of which the end $e$ is connected to busbar $i$ [MW]
$\theta_{l,e}$	Angle of the voltage of line $l$ at end $e$ [rad]
$\theta_{b,i}$	Angle of the voltage at busbar $i$ in substation $b$ [rad]

$\theta_{l,e,i}$	Angle of the voltage at busbar $i$ associated with end $e$ of transmission line $l$ [rad]
$\Delta b_l$	Susceptance change of the line $l$ [S]
$C^{Gen}$	Total generation cost [\$]
$C^{LS}$	Load shedding cost based on $VOLL$ [\$]
$C^{Obj}$	Total operating cost, i.e., $C^{Gen} + C^{LS}$ [\$]

#### Binary Variables

$h_b$	Binary variable indicating the connection status of the two busbars in substation $b$ . (0: disconnected; 1: connected)
$h_g$	Binary variable indicating the busbar connection status of the generator on line $l$ . (0: Busbar 1; 1: Busbar 2)
$h_d$	Binary variable indicating the busbar connection status of the load demand on line $l$ . (0: Busbar 1; 1: Busbar 2)
$h_{l,e}$	Binary variable indicating the busbar connection status of transmission line $l$ 's end $e$ . (0: Busbar 1; 1: Busbar 2)
$h_l$	Binary variable indicating the switching status of transmission line $l$ . (0: open; 1: closed)

## I. Introduction

### A. Motivation

The bulk power system is undergoing a massive transformation driven by the large-scale integration of intermittent renewable energy resources (RERs), inverter-based resources (IBRs) [1], and the rapid growth of data center loads [2]. These developments introduce new operational challenges such as power flow congestion, voltage quality and stability issues [3], [4] and introduces new challenges to the power system utilities to ensure the reliability of the power system. Conventional solutions to these challenges are to expand transmission capacity through new line construction or infrastructure upgrades [5], [6], deploy energy storage systems (ESS) [7], [8], etc. However, these approaches are often capital-intensive and time-consuming, requiring several years for planning, permitting, and commissioning.

In recent years, several Grid Enhancing Technologies (GETs) have emerged as promising alternatives to improve network flexibility and mitigate congestion issues [9], [10], [11]. These include Network Topology Optimization (NTO) [12], [13], [14], Dynamic Line Rating (DLR) [14], [15], and Variable Impedance Devices (VIDs), also referred to as Smart Wire Devices (SWDs) [16], [17]. NTO seeks to optimize both the network topology and the breaker configurations, often represented by the node-breaker model, to enhance operational flexibility. Prior studies [14] have shown that NTO can significantly reduce operational costs compared to fixed-topology systems. Moreover, DLR dynamically adjusts the thermal limits of transmission

lines based on real-time ambient weather conditions, allowing operators to utilize increased line capacity during favorable cooling conditions such as low temperatures and high wind speeds [15]. Meanwhile, VIDs (or SWDs) can modulate the line impedance, effectively rerouting power flows from overloaded lines to underutilized ones [17]. Recognizing the potential of these technologies, the U.S. Department of Energy (DOE) has recently emphasized the importance of GET deployment to enhance grid reliability and flexibility [9]. However, most existing methods address these technologies independently, without considering their interactions or coordination in congestion management. To address this gap, this work proposes a co-optimization framework that jointly models and coordinates NTO, DLR, and distributed VIDs, enabling synergistic operation to alleviate transmission congestion and improve overall system efficiency.

### B. Existing literature

In the existing literature, the optimization of GETs across various operational time horizons has been widely investigated. Recent studies have examined the combined application of Optimal Transmission Switching (OTS) and DLR technologies [18], [19]. These works have demonstrated that integrating OTS and DLR schemes can significantly enhance renewable energy accommodation and improve overall system reliability. In [13], a DLR along with NTO framework, combining OTS and bus-bar splitting, was proposed, showing substantial improvements in system reliability and notable reductions in operational costs.

Moreover, incorporating VIDs into operational planning introduces additional nonlinearities in both the optimal power flow (OPF) and switching problems, as VIDs are typically modeled through variable line impedance [17], [20]. The operation of VIDs has been investigated for several objectives, including congestion management [20], cost minimization, and wind power curtailment reduction [21]. In addition, [22], [23], [24] developed stochastic planning and operational frameworks for the deployment of VIDs under uncertainty.

Overall, the existing body of work has predominantly focused on the individual optimization of specific GETs, with limited attention to their coordinated or co-optimized operation. For instance, while [13] explored the integration of DLR within an NTO framework, and [22] considered VID deployment alongside generator dispatch scheduling, the joint optimization of multiple GETs remains largely unexplored. Consequently, there is a clear research gap in developing unified frameworks that enable the coordinated operation of multiple GETs to fully leverage their combined flexibility and enhance system performance.

### C. Problem Statement and Contributions

In this work, we propose a co-optimization framework for the coordinated operation of multiple GETs. While

previous studies have primarily focused on individual GETs in isolation, our framework simultaneously considers three complementary technologies: NTO, DLR, and VIDs, to exploit their synergistic capabilities in improving power system flexibility and operational efficiency.

First, the network topology and bus-bar splitting are modeled using the node-breaker representation, which enables detailed switching decisions while maintaining network connectivity and operational feasibility. Second, VIDs are incorporated to provide additional flexibility by allowing controlled adjustments of line reactances within predefined operating limits, thereby redistributing power flows and alleviating congestion. Third, DLR is modeled as functions of real-time or forecasted weather conditions, primarily wind speed and ambient temperature, enabling adaptive utilization of transmission capacity based on prevailing environmental factors. The DC power flow model is adopted to represent power flow physics, extended to account for the variable line reactances introduced by the VIDs.

The key contribution of this work lies in the development of a co-optimization scheme that jointly considers NTO, DLR, and VID technologies within a single, integrated decision-making framework. This unified approach enables a systematic assessment of the interactions and combined benefits of multiple GETs under diverse operating and weather conditions. Through this framework, we can evaluate how coordinated control of these technologies enhances network flexibility, increases renewable energy accommodation, and improves overall system reliability, outcomes that are difficult to achieve when each technology is optimized independently.

The paper is organized as follows. Section II presents the model of the grid and GETs. Section III presents the co-optimization framework for the coordination of the multiple GETs. Section IV presents the simulation setup and results on two different IEEE testcases, and Finally, Section V concludes the main contribution of the presented work.

## II. Modeling Grid Enhancing Technologies

In the following, we describe the grid model and the models of different GETs, which will be used later for the co-optimization framework in Sec. III.

### A. Transmission grid model

We model the transmission network using the DC power flow approximation [25], which assumes that (i) the angle of the voltage difference is small, (ii) the network is reactive, and (iii) the voltage magnitudes are close to 1 per unit. Using the notations described in nomenclature section, the DC power flow is expressed as follows.

$$P_l = b_l(\theta_{l,fr} - \theta_{l,to}) \quad (1)$$

Here,  $b_l = \bar{b}_l$ , i.e., when impedances are not controlled.

### B. Network Topology Optimization Model

NTO involves optimizing the configuration of the power network through optimal transmission switching and by leveraging existing switching elements within substations, such as circuit breakers (CBs). The substation CBs enable reconfiguration of substation connections to the rest of the power system, thereby influencing the operational flexibility, reliability, and security of the grid. Substations can employ various bus configurations that require different numbers of circuit breakers and exhibit distinct reliability characteristics. Among these, the breaker-and-a-half configuration is commonly used in high-voltage substations due to its favorable balance between reliability and operational flexibility [26].

In this work, we assume that the node-breaker (NB) model is adopted at each bus in the power network. Figure 1 shows the generalized breaker-and-half model with line switching. As shown in the figure, this model adds additional flexibility that the power system could benefit from, for example, using the NB model, the busbars of the “from” and “to” buses can be either closed or open, and also the connection to the loads and generators can be connected to either of the busbars.

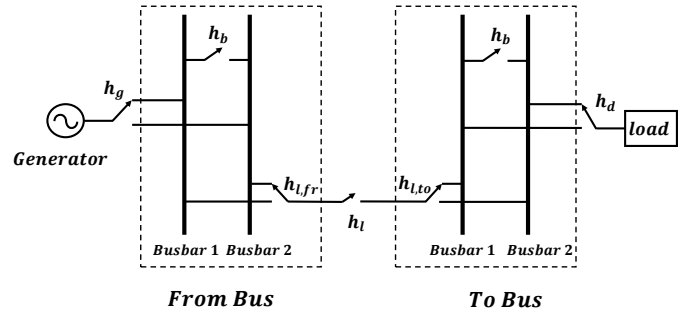


Fig. 1. Generalized breaker-and-half model

Considering the switching capability of the busbars and the lines, the NTO model can be mathematically modeled using busbar binary variables  $h_b$  [13], [14]:

$$-\theta^{max}(1 - h_b) \leq \theta_{b,1} - \theta_{b,2} \leq \theta^{max}(1 - h_b) \quad \forall b \quad (2a)$$

In (2a), when busbars are merged, the difference in voltage angle phase between busbars must be identical, and when split, it must not exceed the maximum angle phase.

The generators connected at each busbars can be modeled using binary variables  $h_g$ , and can be expressed as

$$(1 - h_g)P_g^{min} \leq P_{g,1} \leq (1 - h_g)P_g^{max} \quad \forall g \quad (2b)$$

$$h_g P_g^{min} \leq P_{g,2} \leq h_g P_g^{max} \quad \forall g \quad (2c)$$

where, Eqs. (2b) and (2c) models when a generator is connected to busbar 1 or at busbar 2, and vice versa.

Similarly, the connection and controllability of the demand at each of the busbars are modeled using binary variable  $h_d$  using (2d) as

$$0 \leq P_{d,1} \leq (1 - h_d)P_d^{max} \quad \forall d \quad (2d)$$

$$0 \leq P_{d,2} \leq h_d P_d^{max} \quad \forall d \quad (2e)$$

The limit on the power-flow for each line and the switching of the lines are expressed as

$$-(1 - h_{l,e})P_l^{max} \leq P_{l,e,1} \leq (1 - h_{l,e})P_l^{max} \quad \forall l, e \quad (2f)$$

$$-h_{l,e}P_l^{max} \leq P_{l,e,2} \leq h_{l,e}P_l^{max} \quad \forall l, e \quad (2g)$$

$$-h_l P_l^{max} \leq P_{l,e,1} \leq h_l P_l^{max} \quad \forall l, e \quad (2h)$$

$$h_{l,e} \leq h_l \quad \forall l, e \quad (2i)$$

$$P_l = P_{l,e,1} + P_{l,e,2} \quad \forall l, e \quad (2j)$$

where, Eqs. (2f) and (2g) define the transmission line constraints: when a line is connected to busbar 1, the power flow to the other busbars must be zero, and vice versa. Eqs. (2h) and (2i) specify the line status, ensuring that no power flows when the line is open. Constraint (2j) enforces power conservation by requiring that the total power flowing out of a busbar equals the power flowing from the ‘from’ bus to the ‘to’ bus.

The line switching constraints are expressed using the big- $M$  method, given by (2k), (2l), and (2m)

$$-M(1 - h_l) \leq b_l(\theta_{l,fr} - \theta_{l,to}) - P_l \leq M(1 - h_l) \quad \forall l \quad (2k)$$

$$-h_{l,e}\theta^{max} \leq \theta_{l,e} - \theta_{l,e,1} \leq h_{l,e}\theta^{max} \quad \forall l, e \quad (2l)$$

$$-(1 - h_{l,e}\theta^{max}) \leq \theta_{l,e} - \theta_{l,e,2} \leq h_{l,e}\theta^{max} \quad \forall l, e \quad (2m)$$

The binary variables for busbars, generator, demand connections and lines are connected through Eqs. (2n), (2o), and (2p). When the busbars at each substation are connected, it is not necessary to consider the binary variable determining the connection of the generator, load, and end of the line.

$$h_b + h_g \leq 1 \quad \forall b, g \in G_b \quad (2n)$$

$$h_b + h_d \leq 1 \quad \forall b, d \in D_b \quad (2o)$$

$$h_b + h_{l,e} \leq 1 \quad \forall b, e, l \in LF_b \text{ or } l \in LT_b \quad (2p)$$

Finally, the constraints (2q) and (2r) express the power balance constraints, i.e., the difference between generation and demand is equal to the sum of power flowing through the lines.

$$\sum_{g \in G_b} P_{g,1} - \sum_{d \in D_b} P_{d,1} - \sum_{l \in LF_b} P_l + \sum_{l \in LT_b} P_l = 0 \quad \forall b \quad (2q)$$

$$\sum_{g \in G_b} P_{g,2} - \sum_{d \in D_b} P_{d,2} - \sum_{l \in LF_b} P_l + \sum_{l \in LT_b} P_l = 0 \quad \forall b \quad (2r)$$

### C. Dynamic Line Rating Model

We also consider the dynamic line rating capability in our optimization scheme as one of the GETs. Compared to the static line rating (SLR), which operates by fixing transmission capacity, DLR enables more economical

power system operation by providing higher transmission capacity.

The DLR is modeled based on weather data and follows the IEEE Standard 738-2023 [27]. With notations defined in the nomenclature, the dynamic thermal balance of a conductor can be expressed as

$$\frac{dT_{avg}}{dt} = \frac{1}{mC_p} [R(T_{avg})I^2 + q_s - q_c - q_r] \quad (3a)$$

where  $q_s$ ,  $q_c$ , and  $q_r$  denote the solar heat gain, convective heat loss, and radiative heat loss, respectively. As the ambient temperature rises,  $q_c$  and  $q_r$  decrease, reducing cooling efficiency and current capacity. In contrast, higher wind speed enhances convective heat loss ( $q_c$ ), which cools the conductor more effectively and increases the allowable current. Overall, ambient temperature and wind speed are the dominant weather factors determining the dynamic line rating.

By neglecting the dynamic term  $\frac{dT_{avg}}{dt}$ , the steady-state condition of the thermal balance yields.

$$I = \sqrt{\frac{q_c + q_r - q_s}{R(T_{avg})}} \quad (3b)$$

This simplified steady-state formulation allows for efficient estimation of the allowable current using forecasted weather conditions [28].

Using the DLR,  $P_l^{max}$  in (2f), (2g), and (2j) are updated considering the wind and temperature forecasts. It is updated as

$$P_l^{max} = P_l^{max,DLR} = P_l^{max,SLR} \times \alpha^{DLR} \quad (4)$$

Here,  $\alpha^{DLR}$  is a coefficient representing the ratio of the current when DLR is applied to that under SLR. To determine  $\alpha^{DLR}$ , forecasted ambient temperature and wind speed are used to compute  $q_s$ ,  $q_c$ , and  $q_r$ , and subsequently the allowable current  $I^{DLR}$  from (3b). For comparison, the same procedure is applied to the SLR case, but with fixed ambient conditions of 40°C and 0.5 m/s wind speed, representing the worst-case scenario [27]. The resulting currents  $I^{DLR}$  and  $I^{SLR}$  are then converted into the corresponding power limits  $P_l^{max,DLR}$  and  $P_l^{max,SLR}$ , and their ratio defines  $\alpha^{DLR}$ . A higher temperature or lower wind speed results in a smaller  $\alpha^{DLR}$ , whereas a lower temperature or higher wind speed yields a larger  $\alpha^{DLR}$ .

### D. Variable Impedance Devices Model

VIDs are a type of flexible AC transmission system (FACTS). They are modeled as several kinds of FACTS devices, including Thyristor Controlled Series Compensators (TCSCs), Static Synchronous Series Compensators (SSSCs), and Unified Power Flow Controllers (UPFCs) and are typically modeled through reactances that can be varied by pre-defined limits. The variable impedance/reactance allows flexibility in the transmission

network to re-route the power-flows and help avoid congestion and reduce costs. It can be mathematically modeled as [17], [20], [29]

$$b_l = \bar{b}_l + \Delta b_l \quad (5a)$$

$$-r\bar{b}_l \leq \Delta b_l \leq r\bar{b}_l \quad \forall l, \quad (5b)$$

where,  $\bar{b}_l$  denotes the nominal susceptance and  $\Delta b_l$  is a variable allowing deviations in the line susceptance is bounded by a factor  $r \leq 1$  of nominal susceptance  $\bar{b}_l$ .

### III. Co-optimization Framework

We formulate a co-optimization problem that jointly coordinates the operation of multiple GETs, aiming to minimize the total operating cost while satisfying the respective constraints of each technology. The objective function and its cost components are described below.

#### A. Objective function

The proposed optimization aims to minimize the total system operating cost, which consists of (i) generation cost ( $C^{Gen}$ ) and (ii) load-shedding cost ( $C^{LS}$ ). Each cost component is defined as follows.

1) Generation cost: Generation costs are modeled as a quadratic function, as shown in Equation (6a), and the total generation is determined by the sum of the generation produced at the two busbars.

$$C^{Gen} = \sum_{g=1}^{N_g} (c_{g,2}(P_{g,1} + P_{g,2})^2 + c_{g,1}(P_{g,1} + P_{g,2}) + c_{g,0}) \quad (6a)$$

2) Load shedding cost: The load shedding cost can be calculated as shown in Equation (6b). When transmission capacity constraints fail to meet the total load demand, load shedding may occur. Multiplying the load shedding power by a high-cost  $VOLL$  minimizes the load shedding cost.

$$C^{LS} = VOLL \sum_{b=1}^{N_b} \left( \sum_{d \in D_b} (P_d^{max} - (P_{d,1} + P_{d,2})) \right) \quad (6b)$$

#### B. Final Optimization Problem

The final optimization for coordinating the operation of the NTO, DLR and VID can be formulated as

$$\begin{aligned} \min \quad & C^{Obj} = C^{Gen} + C^{LS}, \\ \text{subject to} \quad & (2), (4), (5). \end{aligned} \quad (7)$$

The optimization problem in (7) is non-linear because of the bilinear constraint of VID when (5) is substituted in (2k) and (1). An approach to tackle these bilinear terms is by transforming them, i.e.,  $\Delta b_l \times \theta_{l,fr}$  and  $\Delta b_l \times \theta_{l,to}$  by auxiliary variables, then applying McCormick envelopes [30]. These McCormick envelopes transform the bilinear constraints to a set of linear constraints by defining upper and lower bounds on each of the variables in the bilinear term. In this work, we do not explicitly reformulate the

bilinear terms using McCormick envelopes; rather, they are typically transformed by the Gurobi optimization solver at the pre-solve stage<sup>1</sup>.

## IV. Simulation Setup and Results

### A. Simulation Setup

We simulate our framework on two different IEEE benchmark test systems which are Case24\_ieee\_rts System and Case 118 system [31], and will be described in the results section. We used the dataset from the MATPOWER testcases for the simulations. In the IEEE test cases, we set the minimum output of all generators to zero in order to avoid situations where a generator's minimum output would exceed the load at its corresponding bus. For the simulations with VIDs, we allow the susceptance change factor (5b),  $r$  to 0.1, allowing each line susceptance to vary by 10%. The cost of load shedding ( $VOLL$ ) is set to 2,000 \$/MWh.

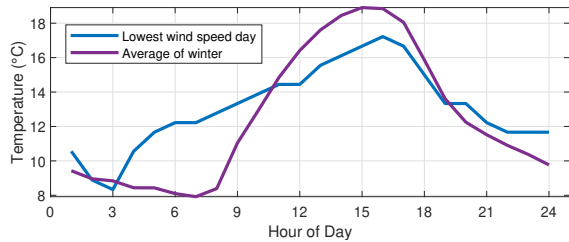
1) Dataset: For simulation, we require the grid data and relevant load data, as well as the weather data to model the DLR. For load data, we use a 24-hour profile with one-hour intervals from [32]. The load for each time period for the considered IEEE testcase is determined by the nominal load data by the normalized hourly profile. The weather data on ambient temperature and wind speed are from Austin, Texas area for the year 2023 [33]. The weather data is used to calculate the  $\alpha^{DLR}$  in (4). All other parameter values were set identically to those for SLR and DLR.

We present results for two cases: (i) High wind: we consider a period when the wind is relatively high and temperature is low. This period is during the winter (December to February). (ii) Low wind: we pick a day during the year characterized with the lowest average wind speed during the year. The average weather data, i.e., for the low wind and high wind cases and corresponding air temperature, are shown in Figure 2. Note that although we consider a low wind day, the wind speed is above 0.5 m/s, which means that it will have a dynamic line rating higher than the static line rating (SLR), and will potentially benefit from the DLR, as will be presented in the results.

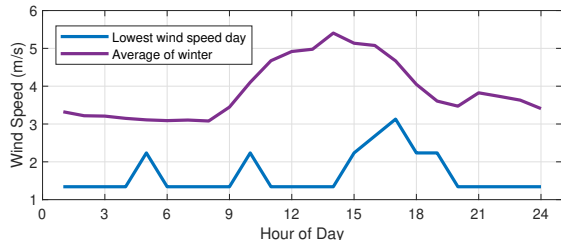
2) Simulation Configuration: The optimization problem was implemented in MATLAB and solved using the Gurobi solver. To study the influence of NTO, VID and DLR, we present simulations for two cases.

(i) Fixed topology: We consider fixed topology, where the operation of the DLR and VID are operation are optimized. In this case, we solve (7) assuming a pre-determined topology representing the base network (i.e., the decisions  $h_l, h_b, h_g$  are already known according to the nominal topology as per the network data).

<sup>1</sup><https://www.gurobi.com/>



(a) Average hourly temperature



(b) Average hourly wind speed

Fig. 2. Weather data on temperature and wind speed for modeling the DLR.

- (ii) Optimized topology: The network topology is optimized using NTO in conjunction with DLR and VID. For the NTO case, the optimization is terminated at a 0.5% optimality gap, as achieving a zero gap requires significantly higher computational time due to the large number of binary decision variables.

Furthermore, to simulate a scenario with a network congestion problem, we first solve a base case without any GETs, then we impose a congestion power-flow limit on each line as half of the base case.

### B. Case24\_ieee\_rts System

Installing DLR or VID technologies requires expensive installation costs [34], [35], therefore, it may not be practical to assume all the transmission lines to be equipped with DLR and VIDs. Therefore, this study applied DLR or VID to only some of the lines instead of applying them to the entire network. The results are then presented for lines with different combinations of DLRs and VIDs. For the following simulations, we incrementally apply the number of transmission lines that are equipped with the DLR and VID technology. The Case24\_ieee\_rts System consists of 38 lines, we increment in steps of 4 lines and simulate for 0, 4, 8, 12, 16 and 20 lines.

1) Fixed Topology: In this case, we solve (7) for the nominal topology, i.e., the decisions  $h_l, h_b, h_g$  are already known according to the nominal topology as per the network data. We present results for low and high wind cases. The results corresponding to the high- and low-wind scenarios are presented in Tables I and II, respectively. Each cell in the table reports the operational cost, denoted as  $C^{\text{Obj}}$  in (7). Each row represents the operational cost for different numbers of VIDs installed across transmission lines, while keeping the number of DLR installations fixed.

Conversely, each column shows the operational cost for varying numbers of DLR-installed lines, with the number of VID installations held constant.

From the results in Tables I and II, the following observations can be deduced from the results.

TABLE I

High Wind Scenario for Fixed Topology: Cost matrix (in  $10^6$ ) for applied DLR and VID lines

# DLR lines	# VID lines					
	0	4	8	12	16	20
0	3.478	3.477	3.169	3.155	3.110	3.083
		(-0.0%)	(-8.9%)	(-9.3%)	(-10.6%)	(-11.4%)
4	3.477	3.464	3.155	3.139	3.093	3.066
		(-0.1%)	(-9.3%)	(-9.8%)	(-11.1%)	(-11.9%)
8	3.141	3.133	3.033	3.014	2.983	2.927
		(-9.7%)	(-9.9%)	(-12.8%)	(-13.4%)	(-15.8%)
12	2.760	2.749	2.533	2.490	2.443	2.412
		(-20.6%)	(-21.0%)	(-27.2%)	(-28.4%)	(-29.8%)
16	2.372	2.360	2.101	2.036	1.947	1.841
		(-31.8%)	(-32.1%)	(-39.6%)	(-41.5%)	(-47.1%)
20	1.955	1.951	1.801	1.761	1.713	1.644
		(-43.8%)	(-43.9%)	(-48.2%)	(-49.4%)	(-52.7%)

TABLE II

Low Wind Scenario for Fixed Topology: Cost matrix (in  $10^6$ ) for applied DLR and VID lines

# DLR lines	# VID lines					
	0	4	8	12	16	20
0	3.478	3.477	3.169	3.155	3.110	3.083
		(-0.0%)	(-8.9%)	(-9.3%)	(-10.6%)	(-11.4%)
4	3.474	3.465	3.156	3.140	3.095	3.067
		(-0.1%)	(-9.3%)	(-9.7%)	(-11.0%)	(-11.8%)
8	3.142	3.135	3.034	3.016	2.986	2.931
		(-9.7%)	(-9.9%)	(-12.8%)	(-13.3%)	(-15.7%)
12	2.849	2.839	2.667	2.638	2.600	2.574
		(-18.1%)	(-18.4%)	(-23.3%)	(-24.1%)	(-26.0%)
16	2.610	2.601	2.419	2.374	2.317	2.243
		(-25.0%)	(-25.2%)	(-30.5%)	(-31.7%)	(-35.5%)
20	2.377	2.370	2.240	2.213	2.168	2.104
		(-31.7%)	(-31.8%)	(-35.6%)	(-36.4%)	(-39.5%)

- In general, DLR has dominant reduction on the operational cost compared to the VIDs. With 20 lines equipped with DLR results in reduction of the operational cost by 43.8%, whereas with 20 lines equipped with VID reduces the cost by only 11.4%. It means that implementing DLR is more effective, but it should be also considered that the effectiveness of DLR technology is directly dependent on the weather. This is reflected in the results with lower wind conditions in Table II, where we notice that the operational cost with DLR reduces by 31.7% which is 12.1% lower than the high wind scenario. However, the effect of VID remains unchanged as it does not depend on the weather conditions.
- The benefit of adding DLR and VID to the transmission lines in steps of 4 reveals that the initial 4 lines do not change much the operational cost, and it might look in the beginning that DLR and VIDs are not

effective. But as we increase their numbers to 8, we see a sudden cost reduction. We observe almost the same level of cost reduction with both DLR and VID up to the number of DLR and VID lines equipped to 8 transmission lines, i.e., 9.7% and 8.9% reduction in DLR and VID, respectively. However, when we consider the cumulative impact of 8 DLR and VID-equipped lines, it results in a cost reduction of 12.8%, so the cost reduction is not necessarily cumulative.

- When the number of DLR-equipped transmission lines are increased, we almost see a linear decrease in the operational costs, whereas for the case VID-equipped lines, the cost reduction is not much significant after 8 lines equipped with VID technology. The linear cost reduction due to DLR continues to when the number of DLR-equipped transmissions lines are increased to 20, whereas for the VID-equipped lines, there is not much improvement in the cost. With this, it can be deduced that there is a limit after which VID technology is not beneficial in reducing the operation cost.
- We can reduce the operational costs by 52.7% and 39.5% for high and low wind scenarios, respectively. Therefore, it can be concluded that DLR and VID technologies are quite effective in reducing the operational costs. We nearly see the cumulative effect of these two technologies, given with 20 lines equipped with VID alone results in an 11.4% reduction in the cost, whereas for DLR, it was 43.8% (in the high wind scenario case).

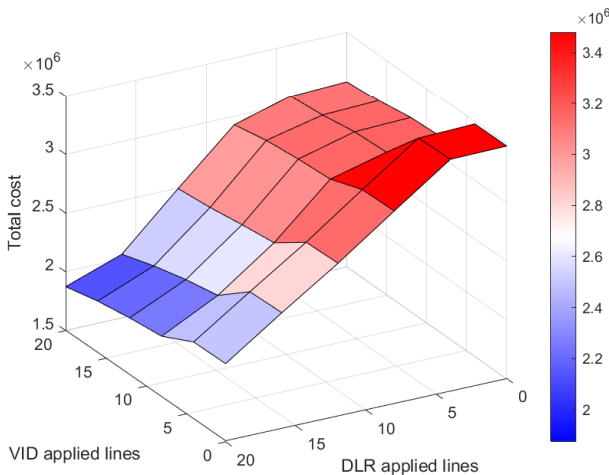


Fig. 3. Average system cost under varying numbers of applied DLR and VID lines (fixed topology).

Figure 3 presents the average of high and low wind scenario objectives considering different combinations of the transmission lines equipped with VID and DLR technologies. As the number of lines with DLR and VID increases, all objective function values consistently decrease. This trend indicates that both technologies

contribute to mitigating line congestion, thereby reducing load shedding and improving overall system efficiency. In particular, DLR exhibits a more pronounced effect than VID, as it directly increases the thermal limits of transmission lines.

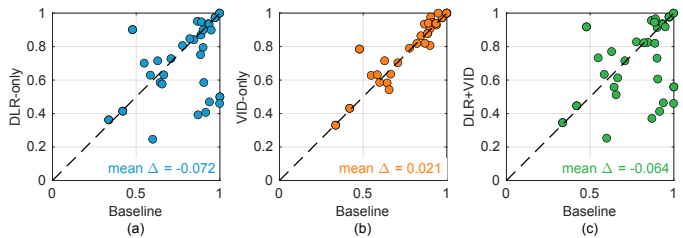


Fig. 4. Comparison of mean line loading between the baseline and (a) DLR-only, (b) VID-only, and (c) DLR+VID. Each dot is a transmission line; axes show line loading (p.u.). The 45° line indicates no change.

We also evaluate how DLR and VID improve the utilization of network resources and thereby reduce operating cost via more economical dispatch and less load shedding. Figure 4 compares the mean line loading between the baseline (no DLR/VID) and three cases: DLR-only, VID-only, and DLR+VID, where each technology is installed on the top eight priority lines. For each transmission line  $\ell$  (38 lines), we use the one-day average  $\bar{u}_\ell = \frac{1}{T} \sum_{t=1}^T |P_\ell(t)| / P_\ell^{\max}(t)$  (p.u.).

With DLR,  $P_\ell^{\max}(t)$  increases according to wind speed and ambient temperature; given these higher limits in the same-day simulation, most points fall below the 45° line (lower mean line loading than baseline), and the average change is negative (e.g.,  $\text{mean } \Delta \bar{u} = -0.072$ ), indicating relieved congestion that enables cheaper generation and less load shedding. With VID, modifying line reactance reroutes power along more economical paths; some lines see higher loading while others decrease, so the scatter remains close to the diagonal with a small average shift (e.g.,  $\text{mean } \Delta \bar{u} = +0.021$ ). When DLR+VID are applied together, both effects appear: a net decrease in mean line loading (e.g.,  $\Delta \bar{u} = -0.064$ ) from DLR’s capacity relief, with additional dispersion due to VID-induced flow redistribution.

2) Optimized Topology through NTO: To evaluate the impact of NTO along with the coordination of DLR and VID technologies, we run the same high and low wind scenarios for Case24\_ieee\_rts System. The corresponding results are presented in Tables III, IV, showing the simulation results when NTO was applied under the same conditions as the fixed topology simulation.

From the results in Tables III and IV, the following observations can be deduced.

- The base cost in the case of optimized topology using NTO (i.e., without any VID and DLRs in the transmission system) is significantly lower than the base cost with fixed topology. Specifically, NTO alone

TABLE III

High Wind Scenario for Optimized Topology using NTO: Cost matrix (in  $10^6$ ) for applied DLR and VID lines

# DLR lines	# VID lines					
	0	4	8	12	16	20
0	2.685	2.685	2.687	2.682	2.682	2.681
		(-0.0%)	(-0.1%)	(-0.1%)	(-0.1%)	(-0.1%)
4	2.034	2.034	2.034	2.034	2.033	2.031
		(-24.2%)	(-24.2%)	(-24.2%)	(-24.3%)	(-24.3%)
8	1.998	1.998	1.998	1.996	1.997	1.994
		(-25.6%)	(-25.6%)	(-25.6%)	(-25.6%)	(-25.7%)
12	1.234	1.234	1.234	1.234	1.234	1.234
		(-54.0%)	(-54.0%)	(-54.0%)	(-54.0%)	(-54.0%)
16	1.229	1.230	1.230	1.230	1.230	1.230
		(-54.2%)	(-54.2%)	(-54.2%)	(-54.2%)	(-54.2%)
20	1.196	1.197	1.197	1.197	1.197	1.197
		(-55.4%)	(-55.4%)	(-55.4%)	(-55.4%)	(-55.4%)

TABLE IV

Low Wind Scenario for Optimized Topology using NTO: Cost matrix (in  $10^6$ ) for applied DLR and VID lines

# DLR lines	# VID lines					
	0	4	8	12	16	20
0	2.685	2.685	2.687	2.682	2.682	2.681
		(-0.0%)	(-0.1%)	(-0.1%)	(-0.1%)	(-0.1%)
4	2.034	2.034	2.034	2.033	2.032	2.031
		(-24.2%)	(-24.2%)	(-24.3%)	(-24.3%)	(-24.4%)
8	2.004	2.004	2.004	2.003	2.002	2.001
		(-25.4%)	(-25.3%)	(-25.4%)	(-25.4%)	(-25.5%)
12	1.278	1.279	1.279	1.279	1.278	1.278
		(-52.4%)	(-52.3%)	(-52.4%)	(-52.4%)	(-52.4%)
16	1.241	1.241	1.241	1.240	1.241	1.241
		(-53.8%)	(-53.8%)	(-53.8%)	(-53.8%)	(-53.8%)
20	1.220	1.220	1.220	1.219	1.219	1.220
		(-54.6%)	(-54.5%)	(-54.6%)	(-54.6%)	(-54.6%)

reduces the operation cost by 22.8% (from  $3.478 \times 10^6$  to  $2.685 \times 10^6$ ).

- When applying NTO, the objective function value did not change based on whether VID was applied, unlike with fixed topology. Optimizing the topology had already significantly reduced the objective function, so applying VID may not be able to further reduce the cost. In some cases, the objective function increased with the VID application, but this result is due to an optimality gap of 0.5% and can be disregarded. However, this observation might be system-dependent.
- We achieve an accumulative reduction in the operation cost by 65.6% and 64.9% for high and low wind scenarios, respectively, using NTO, DLR, and VID applied to 20 transmission lines.

Furthermore, Fig. 5 presents the average of high and low wind scenario objectives considering different combinations of the transmission lines equipped with VID and DLR technologies. According to the plot, the objective function value is significantly reduced by whether DLR is applied. However, it is not affected by the application of VID, indicating that it shows an almost constant value regardless of VID application.

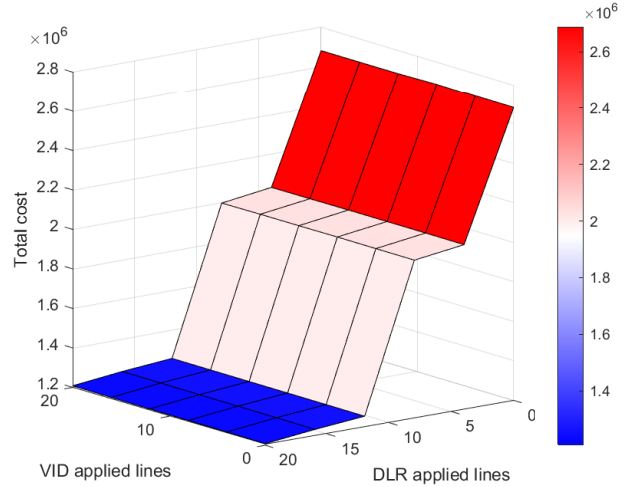


Fig. 5. Average system cost under varying numbers of applied DLR and VID lines (optimized topology using NTO).

### C. Case 118 System

We also validate the proposed algorithm on a larger network: case 118 [31], which consists of 186 lines. We present the results for the case with 60 lines equipped with VID and DLR technologies. We simulate for both the high, and low wind cases and the corresponding results are presented in Table V. The simulation was conducted at 6-hour intervals by calculating the average of weather data and load data every six hours from the single day's data. The objective function for the whole day was calculated by multiplying it by six.

TABLE V  
Cost comparison with NTO, DLR and VIDs under the low and high wind cases. (Case 118 system)

Method	Low wind	High wind
Fixed topology	6,032,010	6,032,010
Fixed topology + DLR	5,030,689 (-16.6%)	4,863,346 (-19.4%)
Fixed topology + VID	5,817,897 (-3.6%)	5,817,897 (-3.6%)
Fixed topology + DLR + VID	4,929,413 (-18.3%)	4,782,459 (-20.7%)
NTO	5,311,093 (-12.0%)	5,311,093 (-12.0%)
NTO + DLR	4,334,524 (-28.1%)	4,186,034 (-30.6%)
NTO + VID	5,309,058 (-12.0%)	5,309,058 (-12.0%)
NTO + DLR + VID	4,333,579 (-28.2%)	4,183,152 (-30.7%)

As it can be observed, NTO, DLR, and VID alone reduce the cost of operation by 12%, 19.4% and 3.6% respectively for the high wind scenario. The cost reduction percentage for DLR alone reduces to 16.6% for the low wind scenario. This suggests that NTO alone is most effective. When all the GETs are used, i.e., NTO+DLR+VID, we can reduce the operation cost by 28.2% and 30.7% in the low and high wind scenarios, respectively. Again, the influence of adding VID is almost negligible when used together with NTO, whereas VID contributed to the case of fixed topology. Overall, these results motivate the use

of co-optimization techniques as the combination of GETs (NTO, DLR, and VIDs) has a significant impact on the net cost reduction.

#### D. Computational performance

We also present the computational performance of the developed algorithm, which is run on a workstation with specifications as Intel(R) Core(TM) Ultra 5 235 (3.40 GHz), RAM: 32.0GB. The table shows the simulation time required for each Case24\_ieee\_rts System and Case 118 system. The computation time for each case is shown in the Table VI. As it can be seen, simulations with fixed topology are quite fast with and without VID, whereas the combination of bilinear terms (due to VID) and binary variables drastically increases the computation time.

TABLE VI

Computational time comparison for different systems and methods for per-hour Simulation.

System	Method	Computational time (s)
Case24_ieee_rts	Fixed topology	0.48
	Fixed topology + DLR + VID	0.97
	NTO	2.75
	NTO + DLR + VID	286.29
Case 118	Fixed topology	1.06
	Fixed topology + DLR + VID	2.44
	NTO	93.33
	NTO + DLR + VID	922.13

#### V. Conclusion

This work presented a co-optimization framework that coordinates different grid enhancing technologies, such as network topology optimization, variable impedance devices, and dynamic line rating - equipped transmission lines with an objective to minimize the operation cost. The problem included bilinear constraints due to variable impedance in the topology optimization model, making it a mixed integer non-linear problem. The optimization problem is solved for two IEEE test cases: case 24 and case 118, and for different wind conditions.

The simulation results on case 24 indicate that DLR alone (on 20 out of 38 lines) is quite effective in improving the operation cost, reducing the cost in the range of 40-50 %. With VID alone (on 20 out of 38 lines), the operation cost can be reduced by 11.4%, and with NTO alone, the operation cost can be reduced by 22.8%. We observed that combining all the technologies, i.e., NTO, DLR, and VID, is able to reduce the operation cost up to 65%, which is quite significant. For the case 118, we observed a cost reduction of almost 30% with NTO and VID, and DLR applied on 50 out of 186 lines. These results demonstrate the effectiveness of the proposed scheme in coordinating different grid-enhancing technologies.

Future work will focus on improving the computational performance of the proposed algorithm by explicitly linearizing the non-linear terms with feasibility and optimality guarantees. The obtained results also motivate

for optimal sizing and placements of the grid-enhancing technologies.

#### References

- [1] Y. Lin, J. H. Eto, B. B. Johnson, J. D. Flicker, R. H. Lasseter, H. N. V. Pico, G.-S. Seo, B. J. Pierre, A. Ellis, J. Miller et al., "Pathways to the next-generation power system with inverter-based resources: Challenges and recommendations," *IEEE Electrification Magazine*, vol. 10, no. 1, pp. 10–21, 2022.
- [2] U.S. Department of Energy, "Evaluating the reliability and security of the united states electric grid," July, 2025. [Online]. Available: <https://www.energy.gov/sites/default/files/2025-07/DOE%20Final%20EO%20Report%20%28FINAL%20JULY%207%29.pdf>
- [3] X. Liang, "Emerging power quality challenges due to integration of renewable energy sources," *IEEE Transactions on Industry Applications*, vol. 53, no. 2, pp. 855–866, 2016.
- [4] North American Electric Reliability Corporation., "Characteristics and risks of emerging large loads - large loads task force white paper," July, 2025. [Online]. Available: [https://www.nerc.com/comm/RSTC\\_Reliability\\_Guidelines/Whitepaper%20Characteristics%20and%20Risks%20of%20Emerging%20Large%20Loads.pdf](https://www.nerc.com/comm/RSTC_Reliability_Guidelines/Whitepaper%20Characteristics%20and%20Risks%20of%20Emerging%20Large%20Loads.pdf)
- [5] C. Lee, S. K. Ng, J. Zhong, and F. F. Wu, "Transmission expansion planning from past to future," in 2006 IEEE PES power systems conference and exposition. IEEE, 2006, pp. 257–265.
- [6] S. De La Torre, A. J. Conejo, and J. Contreras, "Transmission expansion planning in electricity markets," *IEEE transactions on power systems*, vol. 23, no. 1, pp. 238–248, 2008.
- [7] P. Denholm, E. Ela, B. Kirby, and M. Milligan, "Role of energy storage with renewable electricity generation," National Renewable Energy Lab.(NREL), Golden, CO (United States), Tech. Rep., 2010.
- [8] R. Piansky, R. Gupta, and D. K. Molzahn, "Optimizing battery and line undergrounding investments for transmission systems under wildfire risk scenarios: A benders decomposition approach," *Sustainable Energy, Grids and Networks*, p. 101838, 2025.
- [9] U.S. Department of Energy., "Grid-enhancing technologies: Unlocking the full potential of transmission capacity," 2021. [Online]. Available: <https://www.energy.gov/gdo/grid-enhancing-technologies>
- [10] O. Mirzapour, X. Rui, and M. Sahraei-Ardakani, "Grid-enhancing technologies: Progress, challenges, and future research directions," *Electric Power Systems Research*, vol. 230, p. 110304, 2024.
- [11] T. Su, J. Zhao, A. Gomez-Exposito, Y. Chen, V. Terzija, and J. P. Gentle, "Grid-enhancing technologies for clean energy systems," *Nature Reviews Clean Technology*, vol. 1, no. 1, pp. 16–31, 2025.
- [12] R. Bacher and H. Glavitsch, "Network topology optimization with security constraints," *IEEE Transactions on Power Systems*, vol. 1, no. 4, pp. 103–111, 2007.
- [13] M. Heidarifar and H. Ghasemi, "A network topology optimization model based on substation and node-breaker modeling," *IEEE Transactions on Power Systems*, vol. 31, no. 1, pp. 247–255, 2016.
- [14] R. Xiao, Y. Xiang, L. Wang, and K. Xie, "Power system reliability evaluation incorporating dynamic thermal rating and network topology optimization," *IEEE Transactions on Power Systems*, vol. 33, no. 6, pp. 6000–6012, 2018.
- [15] U.S. Department of Energy., "Dynamic line rating - report to congress," 2019. [Online]. Available: [https://www.energy.gov/sites/prod/files/2019/08/f66/Congressional\\_DLR\\_Report\\_June2019\\_final\\_508\\_0.pdf](https://www.energy.gov/sites/prod/files/2019/08/f66/Congressional_DLR_Report_June2019_final_508_0.pdf)
- [16] F. Kreikebaum, D. Das, Y. Yang, F. Lambert, and D. Divan, "Smart wires—a distributed, low-cost solution for controlling power flows and monitoring transmission lines," in 2010 IEEE PES Innovative Smart Grid Technologies Conference Europe (ISGT Europe). IEEE, 2010, pp. 1–8.

- [17] M. Sahraei-Ardakani and K. W. Hedman, "Computationally efficient adjustment of facts set points in dc optimal power flow with shift factor structure," *IEEE Transactions on Power Systems*, vol. 32, no. 3, pp. 1733–1740, 2016.
- [18] R. Xiao, Y. Xiang, L. Wang, and K. Xie, "Bulk power system reliability evaluation considering optimal transmission switching and dynamic line thermal rating," in *2016 International Conference on Probabilistic Methods Applied to Power Systems (PMAPS)*. IEEE, 2016, pp. 1–5.
- [19] K. Wu, L. Wang, H. Ha, and Z. Wang, "Dynamic line rating and optimal transmission switching for maximizing renewable energy sources injection with voltage stability constraint," *Applied Energy*, vol. 378, p. 124651, 2025.
- [20] A. Nikoobakht, J. Aghaei, T. Niknam, M. Shafie-khah, and J. P. Catalao, "Smart wire placement to facilitate large-scale wind energy integration: an adaptive robust approach," *IEEE Transactions on Sustainable Energy*, vol. 10, no. 4, pp. 1981–1992, 2018.
- [21] A. Nasri, A. J. Conejo, S. J. Kazempour, and M. Ghandhari, "Minimizing wind power spillage using an opf with facts devices," *IEEE Transactions on Power Systems*, vol. 29, no. 5, pp. 2150–2159, 2014.
- [22] O. Ziaee and F. Choobineh, "Stochastic location-allocation of tcsc devices on a power system with large scale wind generation," in *2016 IEEE Power and Energy Society General Meeting (PESGM)*. IEEE, 2016, pp. 1–5.
- [23] M. Sahraei-Ardakani and K. W. Hedman, "A fast lp approach for enhanced utilization of variable impedance based facts devices," *IEEE Transactions on Power Systems*, vol. 31, no. 3, pp. 2204–2213, 2015.
- [24] Y. Sang, M. Sahraei-Ardakani, and M. Parvania, "Stochastic transmission impedance control for enhanced wind energy integration," *IEEE Transactions on Sustainable Energy*, vol. 9, no. 3, pp. 1108–1117, 2017.
- [25] B. Stott, J. Jardim, and O. Alsaç, "Dc power flow revisited," *IEEE Transactions on Power Systems*, vol. 24, no. 3, pp. 1290–1300, 2009.
- [26] D. Atanackovic, D. McGillis, and F. Galiana, "Reliability comparison of substation designs," *IEEE transactions on power delivery*, vol. 14, no. 3, pp. 903–910, 1999.
- [27] "Ieee standard for calculating the current-temperature relationship of bare overhead conductors," *IEEE Std 738-2023 (Revision of IEEE Std 738-2012)*, pp. 1–56, 2023.
- [28] C.-M. Lai, J. Teh, B. Alharbi, A. AlKassem, A. Aljabr, and N. Alshammari, "Optimisation of generation unit commitment and network topology with the dynamic thermal rating system considering n-1 reliability," *Electric Power Systems Research*, vol. 221, p. 109444, 2023.
- [29] O. Pohl, S. Dalhues, and C. Rehtanz, "Dc-sensitivities for impedance controllers in an agent-based power flow control system," in *2018 IEEE Power & Energy Society Innovative Smart Grid Technologies Conference (ISGT)*, 2018, pp. 1–5.
- [30] A. Mitsos, B. Chachuat, and P. I. Barton, "McCormick-based relaxations of algorithms," *SIAM Journal on Optimization*, vol. 20, no. 2, pp. 573–601, 2009.
- [31] S. Babaeinejadsarookolaee, A. Birchfield, R. D. Christie, C. Coffrin, C. DeMarco, R. Diao, M. Ferris, S. Fliscounakis, S. Greene, R. Huang et al., "The power grid library for benchmarking ac optimal power flow algorithms," *arXiv preprint arXiv:1908.02788*, 2019.
- [32] R. Gupta, F. Sossan, and M. Paolone, "Grid-aware distributed model predictive control of heterogeneous resources in a distribution network: Theory and experimental validation," *IEEE Transactions on Energy Conversion*, vol. 36, no. 2, pp. 1392–1402, 2021.
- [33] National Oceanic and Atmospheric Administration (NOAA), National Centers for Environmental Information (NCEI), "Climate data online (cdo)," 2025, accessed: 2025-09-17. [Online]. Available: <https://www.ncei.noaa.gov/cdo-web/>
- [34] O. Pohl, "Coordination of impedance controllers and flexible power for curative congestion management in real-time applications," Ph.D. dissertation, Dissertation, Dortmund, Technische Universität, 2024, 2024.
- [35] W. Wang and S. Pinter, "Dynamic line rating systems for transmission lines: Topical report," US Department of Energy, Office of Electricity Delivery & Energy Reliability, 2014.